MAGNETOHYDRODYNAMICS NANOFERRO FLUID FLOWS PASSING THROUGH A MAGNETIC POROUS SPHERE UNDER THERMAL RADIATION EFFECT

by Tri Rahayuningsih

Submission date: 22-Sep-2023 10:12AM (UTC+0700)
Submission ID: 2173255648
File name: ilovepdf_merged.pdf (1.12M)
Word count: 4018
Character count: 21021

BAREKENG: Journal of Mathematics and Its Application
December 2022 Volume 16 Issue 4 Page 1303–1312
P-ISSN: 1978-7227 E-ISSN: 2615-3017
https://doi.org/10.30598/barekengvol16iss4pp1303-1312

MAGNETOHYDRODYNAMICS NANOFERRO FLUID FLOWS PASSING THROUGH A MAGNETIC POROUS SPHERE UNDER THERMAL RADIATION EFFECT

Basuki Widodo[1*], Eirene J. Pamela[2], Dieky Adzkiya[3], Chairul Imron[4], Tri Rahayuningsih[5]

[1,2,3,4] Department of Mathematics, Faculty of Science and Data Analytics, Institut Teknologi Sepuluh Nopember
Sukolilo, Surabaya, 60111, Indonesia
[5]Department of Agroindustrial Technology, Universitas Wijaya Kusuma Surabaya
Surabaya, Jawa Timur, 60225, Indonesia

Corresponding author's e-mail: [1] b_widodo@matematika.its.ac.id*

Abstract. *In the application of thermonuclear reactor cooling, temperature regulation relies on experiments based on practical experience. Therefore, the accuracy of this temperature setting is operator-dependent. So it is necessary to develop a mathematical model to solve these problems. The dimensional mathematical model therefore is generated using the conservation laws of mass, momentum, and energy. The dimensional mathematical model is further transformed into non-dimensional mathematical model by using non-dimensional variables. The non-dimensional mathematical model is simplified using the similarity equation by utilizing the stream function. The model obtained is a system of nonlinear ordinary differential equations. This system of equations is then solved using an implicit numerical method using the Keller-Box scheme. This Keller-Box method has high accuracy and is more efficient. The numerical simulation results show that the velocity profile and temperature profile decrease as the magnetic parameter, porosity parameter, and the Prandtl number increase, respectively. Meanwhile, when the radiation parameter increases, the temperature profile also increases, but the radiation parameter does not affect the velocity profile.*

Keywords: *magnetohydrodynamics, nanoferro fluid, porous sphere, thermal radiation.*

Article info:
Submitted: 4th July 2022 *Accepted: 19th October 2022*

How to cite this article:
B. Widodo, E. J. Pamela, D. Adzkiya, C. Imron and T. Rahayuningsih, "MAGNETOHYDRODYNAMICS NANOFERRO FLUID FLOWS PASSING THROUGH A MAGNETIC POROUS SPHERE UNDER THERMAL RADIATION EFFECT", *BAREKENG: J. Math. & App.*, vol. 16, iss. 4, pp. 1303-1312, Dec., 2022.

1. INTRODUCTION

In the application of thermonuclear reactor cooling, we still rely on experiments based on practical experience in regulating temperature. So the accuracy of the temperature setting depends on the operator. Therefore, in this temperature regulation, it is necessary to develop an accurate technique or method based on scientific temperature calculations that are acceptable to all parties and the experience of the operator. In terms of this mathematical model, there has been a preliminary model of temperature regulation. However, further, development is still needed.

In terms of mathematical model, the fluid considered is nanofluid, e.g. ferrofluid. The nanoferro fluid is Newtonian fluid. This nanoferro fluid contains nano-particles (ferroparticles) [1]. The nanoparticle used is Fe_2O_3 with water as the base fluid. Meanwhile, magnetohydrodynamics is a science that studies the flow of fluids that conduct electricity due to magnetic induction in the fluid [2]. The basic concept of magnetohydrodynamics is the induction of a magnetic field capable of conducting electricity in a moving conductive fluid. Thus giving rise to the Lorentz force which exerts a force on the fluid and also changes its own magnetic field [3]. In this paper, we consider the effect of magnetohydrodynamics is caused by the porous sphere's magnetic field and the influence of ferrofluid radiation.

Many studies have been carried out on the magnetohydrodynamic flow of nanoferro fluid on various surfaces, for example, in rectangular channels by Aminfar *et al*. [4], on inclined plates by Ilias *et al*. [5], over a horizontally rotating disk by Shah *et al*. [6], through T-shaped ventilated cavities by Jhumur *et*. *al*. [7], over a cylinder by Reddy *et al*. [8], through a surface that is a non-linear motion by Jamaludin *et*. *al*. [9], as well as through solid spherical surfaces by Widodo *et*. *al*. [10]. From these literatures, it has been mentioned that the volume fraction of air-based ferro particles, thermal radiation, and type parameters are the main factors in increasing heat transfer in nanoferro fluids. We, therefore, develop a mathematical model to solve the magnetohydrodynamics problem of radiative nanoferro fluid flowing over the surface of a porous magnetic sphere.

2. RESEARCH METHODS

In this study, the object (bluff body) considered is a porous magnetic ball, as seen in Figure 1. It is known that nanoferro fluid flows from bottom to top against the direction of gravity and has a speed of U_∞ and a temperature of T_∞ far from the porous magnetic sphere. While T_w is the temperature on the surface of the porous magnetic sphere. x is measured anticlockwise from downward vertical along a sphere surface. The distances x and y are measured respectively to the vertical line through the porous magnetic sphere and to the surface of the porous magnetic sphere [11]. In this study, the focus area is in front of the lower stagnation point of the porous magnetic sphere.

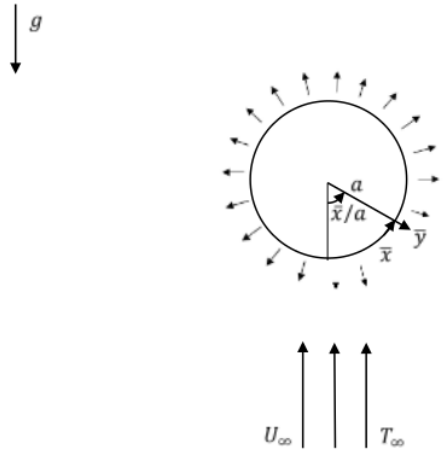

Figure 1. Sketch of a Nanoferro fluid Flow Through a Magnetic Porous Sphere

2.1 Developing Dimensional Equation

In this research, the system is both steady and incompressible. Therefore, the dimensional governing equations of continuity, momentum, and energy equation can be expressed as:

$$\frac{\partial(\bar{r}\bar{u})}{\partial\bar{x}}+\frac{\partial(\bar{r}\bar{v})}{\partial\bar{y}}=0 \tag{1}$$

$$\rho_{ff}\left(\bar{u}\frac{\partial\bar{u}}{\partial\bar{x}}+\bar{v}\frac{\partial\bar{u}}{\partial\bar{y}}\right)=-\frac{\partial\bar{p}}{\partial\bar{x}}+\mu_{ff}\left(\frac{\partial^2\bar{u}}{\partial\bar{x}^2}+\frac{\partial^2\bar{u}}{\partial\bar{y}^2}\right)+\sigma B_0^2\bar{u}+\frac{\mu_{ff}}{K^*}\bar{u}+\rho_{ff}\beta(\bar{T}-T_\infty)g\sin\frac{\bar{x}}{a} \tag{2}$$

$$\rho_{ff}\left(\bar{u}\frac{\partial\bar{v}}{\partial\bar{x}}+\bar{v}\frac{\partial\bar{v}}{\partial\bar{y}}\right)=-\frac{\partial\bar{p}}{\partial\bar{y}}+\mu_{ff}\left(\frac{\partial^2\bar{v}}{\partial\bar{x}^2}+\frac{\partial^2\bar{v}}{\partial\bar{y}^2}\right)+\sigma B_0^2\bar{v}+\frac{\mu_{ff}}{K^*}\bar{v}-\rho_{ff}\beta(\bar{T}-T_\infty)g\cos\frac{\bar{x}}{a} \tag{3}$$

$$\frac{\partial\bar{T}}{\partial\bar{t}}+\bar{u}\frac{\partial\bar{T}}{\partial\bar{x}}+\bar{v}\frac{\partial\bar{T}}{\partial\bar{y}}=\alpha_{ff}\left(\frac{\partial^2\bar{T}}{\partial\bar{x}^2}+\frac{\partial^2\bar{T}}{\partial\bar{y}^2}\right)-\frac{1}{(\rho C_p)_{ff}}\frac{\partial q_r}{\partial\bar{y}} \tag{4}$$

with the boundary conditions
$\bar{u}=\bar{v}=0,\bar{T}=T_w$ at $\bar{y}=0$
$\bar{u}=\bar{u}_e(\bar{x}),\bar{T}=T_\infty$ at $\bar{y}\to\infty$

where $\bar{u}$ and $\bar{v}$ represent the velocity components along the $\bar{x}$ and $\bar{y}$ axes, respectively. Furthermore, the subscripts ff and f refer to ferrofluid and base fluid. Then, $\bar{r}$ is radial distance from the axis of symmetry to the spherical surface, B_0 is the magnetic field, μ is dynamic viscosity, ρ is density, g is the acceleration due to gravity, σ is electrical conductivity, β is ferrofluid thermal expansion, $\bar{T}$ is local temperature, ρC_p is effective heat capacity, and α is heat diffusivity [12]. Furthermore, the Rosseland approximation [13] is used where the radiative heat flux, q_r, is defined

$$q_r=-\frac{4\sigma^*}{3k^*}\frac{\partial T^4}{\partial\bar{y}}$$

where σ^* is the Stefan-Boltzmann constant and k^* represents the average absorption coefficient. The temperature difference around the flow is assumed to be T^4, which can be further extended in the Taylor series as a linear combination of temperatures. Then by expanding T^4 into the Taylor series for T_∞ and ignoring the higher-order terms [14], we obtain $T^4=4T_\infty^3T-3T_\infty^4$. Thus, Equation (4) is reduced to

$$\frac{\partial\bar{T}}{\partial\bar{t}}+\bar{u}\frac{\partial\bar{T}}{\partial\bar{x}}+\bar{v}\frac{\partial\bar{T}}{\partial\bar{y}}=\alpha_{ff}\left(\frac{\partial^2\bar{T}}{\partial\bar{x}^2}+\frac{\partial^2\bar{T}}{\partial\bar{y}^2}\right)+\frac{1}{(\rho C_p)_{ff}}\frac{16\sigma^*T_\infty^3}{3k^*}\frac{\partial^2\bar{T}}{\partial\bar{y}^2} \tag{5}$$

2.2 Non-dimensional Equation

The dimensional equations that have been obtained are further transformed into non-dimensional equations. We apply non-dimensional variables as follows [15]

$$x=\frac{\bar{x}}{a},y=Re^{\frac{1}{2}}\left(\frac{\bar{y}}{a}\right),r=\frac{\bar{r}}{a},u=\frac{\bar{u}}{U_\infty},v=Re^{\frac{1}{2}}\left(\frac{\bar{v}}{U_\infty}\right),p=\frac{\bar{p}}{\rho_{ff}U_\infty^2},T=\frac{\bar{T}-T_\infty}{T_w-T_\infty}$$

Furthermore, the non-dimensional parameters are given as follows [10][15][16]

$$M=\frac{a\sigma B_0^2}{\rho_{ff}U_\infty},\lambda=\frac{Gr}{Re^2},Gr=\frac{g\beta(T_w-T_\infty)a^3}{v_{ff}^2},Pr=\frac{v_f}{\alpha_f},\phi=\frac{a\mu_{ff}}{\rho_{ff}U_\infty K^*},Nr=\frac{4\sigma^*T_\infty^3}{k^*k_f}$$

where M is a magnetic parameter, λ is a convection parameter, Gr is a Grashof number, Pr is a Prandtl number, ϕ is a porosity parameter, and Nr is a radiation parameter. By substituting non-dimensional variables and non-dimensional parameters into Equations (1), (2), (3), and (5), the following non-dimensional equations are obtained as follows,

$$\frac{\partial(ru)}{\partial x}+\frac{\partial(rv)}{\partial y}=0 \tag{6}$$

$$u\frac{\partial u}{\partial x}+v\frac{\partial u}{\partial y}=-\frac{\partial p}{\partial x}+\frac{1}{Re}\frac{v_{ff}}{v_f}\frac{\partial^2u}{\partial x^2}+\frac{v_{ff}}{v_f}\frac{\partial^2u}{\partial y^2}+(M+\phi)u+\lambda T\sin x \tag{7}$$

$$\frac{1}{Re}\left(u\frac{\partial v}{\partial x}+v\frac{\partial v}{\partial y}\right)=-\frac{\partial p}{\partial y}+\frac{1}{Re^2}\frac{v_{ff}}{v_f}\frac{\partial^2 v}{\partial x^2}+\frac{1}{Re}\frac{v_{ff}}{v_f}\frac{\partial^2 v}{\partial y^2}+\frac{1}{Re}Mv+\frac{1}{Re}\phi v-\frac{1}{Re^{\frac{1}{2}}}\lambda T\cos x \quad (8)$$

$$u\frac{\partial T}{\partial x}+v\frac{\partial T}{\partial y}=\frac{1}{PrRe}\frac{\alpha_{ff}}{\alpha_f}\frac{\partial^2 T}{\partial x^2}+\frac{1}{Pr}\frac{\alpha_{ff}}{\alpha_f}\left(1+\frac{4}{3}\frac{k_f}{k_{ff}}Nr\right)\frac{\partial^2 T}{\partial y^2} \quad (9)$$

with the non-dimensional boundary conditions

$u=v=0, T=1$ at $y=0$
$u=u_e(x), T=0$ at $y\to\infty$

Furthermore, the variables related to nanoferro fluid and base fluid are defined as follows [17][18]

$$\rho_{ff}=(1-\chi)\rho_f+\chi\rho_s, \qquad \mu_{ff}=\frac{\mu_f}{(1-\chi)^{2.5}},$$
$$\left(\rho C_p\right)_{ff}=(1-\chi)\left(\rho C_p\right)_f+\chi\left(\rho C_p\right)_s, \qquad \frac{k_{ff}}{k_f}=\frac{\left(k_s+2k_f\right)-2\chi\left(k_f-k_s\right)}{\left(k_s+2k_f\right)+\chi\left(k_f-k_s\right)}$$

where χ is volume fraction. By substituting these variables into Equations (6) to (9) and by using boundary layer theory, then the equation becomes respectively as follows

$$\frac{\partial(ru)}{\partial x}+\frac{\partial(rv)}{\partial y}=0 \quad (10)$$

$$u\frac{\partial u}{\partial x}+v\frac{\partial u}{\partial y}=-\frac{\partial p}{\partial x}+\left(\frac{1}{(1-\chi)^{2.5}\left((1-\chi)+\chi\frac{\rho_s}{\rho_f}\right)}\right)\frac{\partial^2 u}{\partial y^2}+(M+\phi)u+\lambda T\sin x \quad (11)$$

$$0=-\frac{\partial p}{\partial y} \quad (12)$$

$$u\frac{\partial T}{\partial x}+v\frac{\partial T}{\partial y}=\frac{1}{Pr}\left(\frac{\left(k_s+2k_f\right)-2\chi\left(k_f-k_s\right)}{\left[\left(k_s+2k_f\right)+\chi\left(k_f-k_s\right)\right]\left[(1-\chi)+\chi\left(\left(\rho C_p\right)_s/\left(\rho C_p\right)_f\right)\right]}+\frac{4}{3}\frac{1}{(1-\chi)+\chi\left(\left(\rho C_p\right)_s/\left(\rho C_p\right)_f\right)}Nr\right)\frac{\partial^2 T}{\partial y^2} \quad (13)$$

In Equation (12), the pressure p does not depend on the variable y. Thus, the equation for momentum exists in the system only on the x-axis. Furthermore, by defining u_e as the velocity outside the boundary layer, then the momentum equation outside the boundary layer is obtained as follows:

$$u\frac{\partial u}{\partial x}+v\frac{\partial u}{\partial y}=u_e\frac{\partial u_e}{\partial x}+\frac{1}{(1-\chi)^{2.5}\left((1-\chi)+\chi\frac{\rho_s}{\rho_f}\right)}\frac{\partial^2 u}{\partial y^2}+(M+\phi)(u-u_e)+\lambda T\sin x \quad (14)$$

2.3 Similarity Equation

The non-dimensional equations that have been obtained are further converted into similarity equations using the stream function. The stream function simplifies the system of equations making computations easier. To solve the non-dimensional equation, then the variables are defined as follows [19]

$$\psi=xr(x)f(x,\eta), \qquad T=\theta(x,\eta)$$

where $r(x)=\sin x$ and ψ is a flow function expressed as

$$u=\frac{1}{r}\frac{\partial\psi}{\partial\eta} \text{ dan } v=-\frac{1}{r}\frac{\partial\psi}{\partial x}$$

Then substituting the stream function into Equations (10), (13), and (14) respectively, we obtain

$$0=-(f')^2+2ff''+\frac{9}{4}+\frac{1}{(1-\chi)^{2.5}\left((1-\chi)+\chi\frac{\rho_s}{\rho_f}\right)}f'''+(M+\phi)\left(f'-\frac{3}{2}\right)+\lambda\theta \quad (15)$$

$$0=2f\theta'+\frac{1}{Pr}\left(\frac{\left(k_s+2k_f\right)-2\chi\left(k_f-k_s\right)}{\left[\left(k_s+2k_f\right)+\chi\left(k_f-k_s\right)\right]\left[(1-\chi)+\chi\left(\left(\rho C_p\right)_s/\left(\rho C_p\right)_f\right)\right]}+\frac{4}{3}\frac{1}{(1-\chi)+\chi\left(\left(\rho C_p\right)_s/\left(\rho C_p\right)_f\right)}Nr\right)\theta'' \quad (16)$$

with the boundary conditions

$f(0)=f'(0)=0$ and $\theta=1$ at $\eta=0$
$f'(\infty)=1$ and $\theta=0$ at $\eta\to\infty$

2.4 Numerical Solution

The similarity equation that has been obtained is then solved using the Keller-Box method. Using the procedure described by Cebeci and Bradshaw, the steps of this method are as follows [20]:

1. Converting second-order or higher-order equations into first-order differential equations.
2. Discretize by using a finite-difference to the center.
3. Linearize the discretized equation and write it in vector-matrix form.
4. Solve a linear system using the tridiagonal-block-elimination method.

3. RESULTS AND DISCUSSION

The nanoparticles considered in this study is Fe_2O_3 with water as the base fluid. Thermophysical properties of base fluid and ferroparticles are defined in Table 1 [21].

Table 1. Thermophysical Properties

Physical properties	Water	Fe_2O_3
$\rho\ (kg/m^3)$	997.1	5260
$C_p\ (J/kg \cdot K)$	4179	570
$k\ (W/m \cdot K)$	0.613	0.58

The simulation results for each parameter variation are described as follows

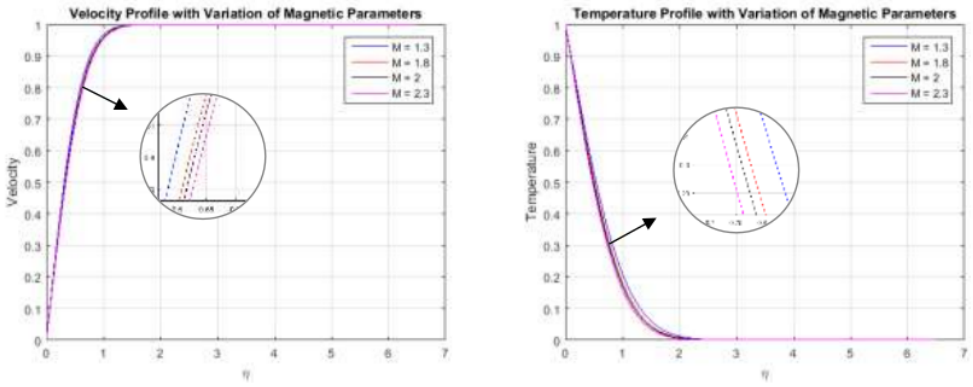

(a) (b)

Figure 2. (a) Velocity Profile and (b) Temperature Profile with Variation of Magnetic Parameters

Figure 2 show the variation of magnetic parameter, namely $M = 1.3, 1.8, 2, 2.3$. Other parameters used are porosity parameter $\phi = 1.04$, Prandtl number $Pr = 1.7$, radiation parameter $Nr = 1$, mixed convection $\lambda = 1$, and volume fraction $\chi = 0.1$. The Magnetic parameters are directly proportional to the electrical conductivity and magnitude of the magnetic field, but are inversely proportional to the density of the fluid. Figure 2(a) shows that the larger the parameters, the lower the velocity profiles of the fluid flow. This is occurred as the existence of Lorentz force on the magnetic ball that causes the fluid passing through the ball to receive the Lorentz force. Since the magnitude of the Lorentz force is proportional to the magnetic parameter, then as the magnetic parameter increases, the Lorentz force also increases. As a result, the Lorentz force around the magnetic sphere also increases, thus affecting the decrease in the velocity of the fluid around the sphere. Further, in Figure 2(b), it shows that the temperature profile in this flow decreases with increasing magnetic parameters. This is due to the decrease in the internal energy of the fluid. The velocity of the fluid that decreases results in an increase in fluid density. As the density of the fluid increases, the heat transfer that occurs will slow down more and more as the magnetic parameters increase.

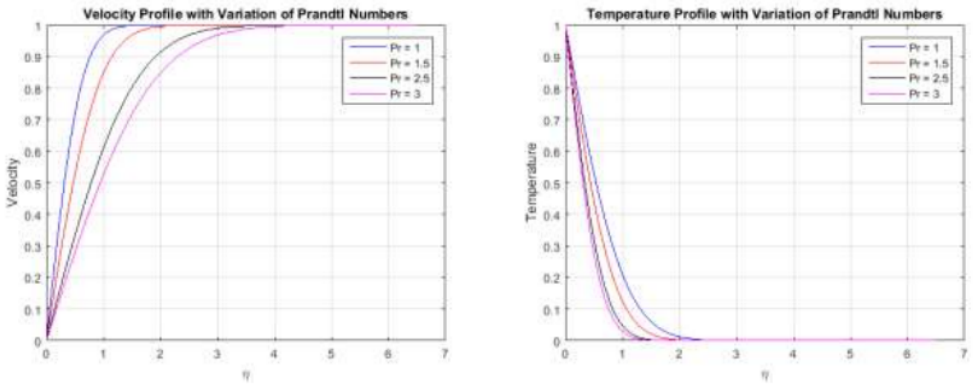

(a) (b)

Figure 3. (a) Velocity Profile and (b) Temperature Profile with Variation of Prandtl Numbers

The Figure 3 depicts the variation of the Prandtl number, namely $Pr = 1, 1.5, 2.5, 3$. Other parameters used are magnetic parameter $M = 1.3$, porosity parameter $\phi = 1$, radiation parameter $Nr = 0.5$, mixed convection $\lambda = 1$, and volume fraction $\chi = 0.1$. Figure 3(a) shows that the greater the Prandtl number, the velocity profile of the fluid flow will decrease. This is occurred because the Prandtl number is inversely proportional to the thermal diffusivity but directly proportional to the kinematics viscosity. Thus, the greater the Prandtl number, the kinematics viscosity in the fluid will also be greater, so that the viscosity of the fluid will increase. As a result, the velocity of the fluid becomes slower or smaller. In Figure 3(b), it further shows that the temperature profile of the fluid decreases with the increase in the Prandtl number. This is because when the Prandtl number increases, the thermal diffusivity decreases, so that the fluid temperature decreases.

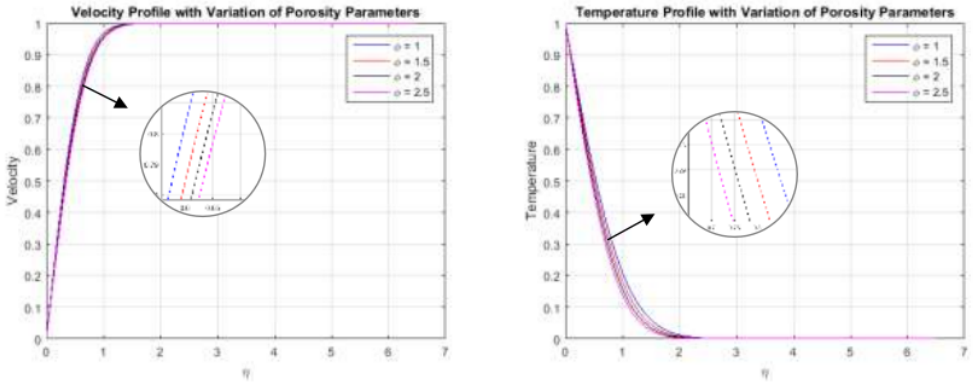

(a) (b)

Figure 4. (a) Velocity Profile and (b) Temperature Profile with Variation of Porosity Parameters

Figure 4 shows the variation of the porosity parameter, namely $\phi = 1, 1.5, 2, 2.5$. Other parameters used are magnetic parameter $M = 1.3$, Prandtl number $Pr = 1$, radiation parameter $Nr = 0.5$, mixed convection $\lambda = 1$, and volume fraction $\chi = 0.1$. Figure 4(a) shows that the greater the porosity parameter, the velocity profile of the fluid flow will decrease. This is occurred because the porosity parameter is directly proportional to the dynamic viscosity but inversely proportional to the density of the fluid. Thus, the greater the porosity parameter, the dynamics viscosity in the fluid will also be greater. As a result, the velocity of the fluid becomes slower or smaller. Further, in Figure 4(b), it shows that the temperature profile of the fluid decreases with increasing porosity parameters. This happens because when the fluid velocity decreases, the resulting skin friction also decreases, so that the fluid temperature decreases.

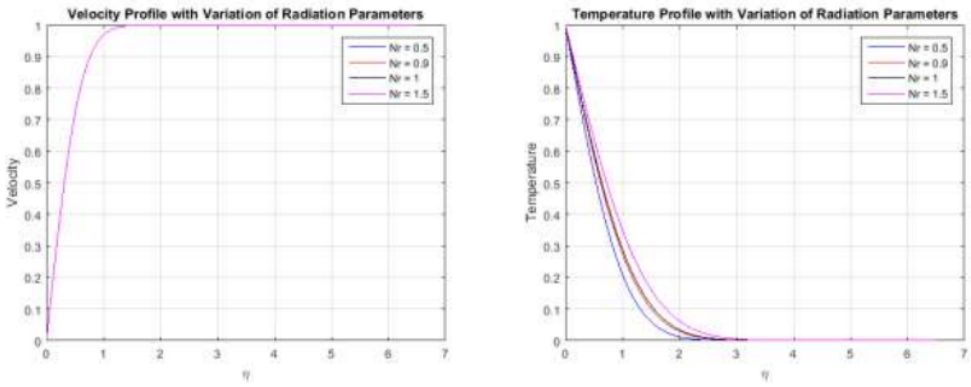

(a) (b)

Figure 5. (a) Velocity Profile and (b) Temperature Profile with Variation of Radiation Parameters

Figure 5 shows the variations of radiation parameters are $Nr = 0.5, 0.9, 1, 1.5$. Other parameters used are magnetic parameter $M = 1.3$, Prandtl number $Pr = 1$, porosity parameter $\phi = 1$, mixed convection $\lambda = 1$, and volume fraction $\chi = 0.1$. Figure 5(a) shows that the radiation parameters have no effect on the velocity profile. This is occurred as radiation dominantly affects the energy equation rather than the momentum equation, so this radiation parameter only affects changes in fluid temperature. Then, in Figure 5(b), it shows that the greater the radiation parameter, the temperature profile of the fluid also increases. This is occurred because the increase in the value of the radiation parameter has a tendency to increase the conduction effect and provide a level of dominance of the heat source, thus causing the fluid temperature increases.

The simulation results are validated with research that has been produced by [22].

4. CONCLUSIONS

Based on the analysis and discussion that has been carried out using several variations of parameters, namely magnetic parameters, Prandtl number, porosity parameters, and radiation parameters on ferrofluid nanoparticles Fe_2O_3, it can be concluded that:

a. When the magnetic parameters increase, the velocity profile and temperature profile decrease. With the variation of magnetic parameters given is $M = 1.3, 1.8, 2, 2.3$.

b. When the Prandtl number increases, the velocity profile and temperature profile decrease. With the given variation of Prandtl numbers is $Pr = 1, 1.5, 2.5, 3$.

c. When the porosity parameters increase, the velocity profile and temperature profile decrease. With the variation of the given porosity parameter is $\phi = 1, 1.5, 2, 2.5$.

d. As the radiation parameters increase, the temperature profile increases, but radiation does not exert an influence on the velocity profile because the dominant radiation affects the energy equation rather than the momentum equation. With variations in the radiation parameters given are $Nr = 0.5, 0.9, 1, 1.5$.

AKNOWLEDGEMENT

This work is based on the research supported by The Ministry of Education, Culture, Research, and Technology/ National Research and Innovation Agency of Indonesian Republic (KEMENDIKBUDRISTEK-RI) with Funding Agreement Letter number 008/E5/PG.02.00.PT/2022, 16th March 2022, and The Directorate

for Research and Community Development (Direktorat Riset dan Pengabdian kepada Masyarakat/DRPM), Institut Teknologi Sepuluh Nopember (ITS) Surabaya-East Java, Indonesia with Funding Agreement Letter number 1503/PKS/ITS/2022, 17th March 2022. We are therefore very grateful to KEMENDIKBUDRISTEK-RI and DRPM-ITS for giving us chance to publish this paper in the Journal of Barekeng-Mathematics Department of Universitas Pattimura Ambon.

REFERENCES

1. K. Raj, and S. Street, "Ferrofluids- Properties and Applications," vol. 8, no. 4, pp. 233–236, 1987. https://analyticalscience.wiley.com/do/10.1002/gitlab.14498
2. R. E. Rosensweig, *Ferrohydrodynamics*. Courier Corporation, 2013. https://books.google.co.id/books?id=ng_DAgAAQBAJ&printsec=frontcover&hl=id&source=gbs_ge_summary_r&cad=0#v=onepage&q&f=false
3. R. Sahaya, B. Widodo, and C. Imron, "Aliran Fluida Magnetohidrodinamik Viskoelatis Tersuspensi yang Melewati Pelat Datar," *J. Sains Dan Seni ITS*, vol. 5, no. 2, pp. 2337–3520, 2016. https://www.semanticscholar.org/paper/Aliran-Fluida-Magnetohidrodinamik-Viskoelatis-yang-Sahaya-Widodo/3109e3c2ef50a8837ceae0cc60e119ad5c4bdcbd
4. H. Aminfar, M. Mohammadpourfard, and S. A. Zonouzi, "Numerical study of the ferrofluid flow and heat transfer through a rectangular duct in the presence of a non-uniform transverse magnetic field," *J. Magn. Magn. Mater.*, vol. 327, pp. 31–42, 2013. https://www.sciencedirect.com/science/article/abs/pii/S0304885312007524
5. M. R. Ilias, N. A. Rawi, and S. Shafie, "Steady aligned MHD free convection of ferrofluids flow over an inclined plate," *J. Mech. Eng.*, vol. 14, no. 2, pp. 1–15, 2017. https://www.researchgate.net/publication/322803039_Steady_aligned_MHD_free_convection_of_ferrofluids_flow_over_an_inclined_plate
6. Z. Shah, A. Dawar, P. Kumam, W. Khan, and S. Islam, "Impact of nonlinear thermal radiation on MHD nanofluid thin film flow over a horizontally rotating disk," *Appl. Sci.*, vol. 9, no. 8, p. 1533, 2019. https://www.mdpi.com/2076-3417/9/8/1533.
7. N. C. Jhumur and S. Saha, "Unsteady MHD mixed convection in a T-shaped ventilated cavity filled with ferrofluid (Fe 3 O 4–water)," *in AIP Conference Proceedings*, vol. 1851, no. 1, p. 20026, 2017. https://aip.scitation.org/doi/10.1063/1.4984655.
8. M. G. Reddy, P. V. Kumari, and P. Padma, "Effect of thermal radiation on MHD casson nano fluid over a cylinder," *J. Nanofluids*, vol. 7, no. 3, pp. 428–438, 2018. https://www.researchgate.net/publication/325500029_Effect_of_Thermal_Radiation_on_MHD_Casson_Nano_Fluid_Over_a_Cylinder.
9. A. Jamaludin, K. Naganthran, R. Nazar, and I. Pop, "Thermal radiation and MHD effects in the mixed convection flow of Fe3O4–water ferrofluid towards a nonlinearly moving surface," *Processes*, vol. 8, no. 1, p. 95, 2020. https://www.mdpi.com/2227-9717/8/1/95.
10. Y. S. H. Mat, M. K. A. Mohamed, Z. Ismail, B. Widodo, and M. Z. Salleh, "Numerical method approach for magnetohydrodynamic radiative ferrofluid flows over a solid sphere surface," *Therm. Sci.*, vol. 25, no. Spec. issue 2, pp. 379–385, 2021. https://www.researchgate.net/publication/361023091_Numerical_Investigation_of_Ferrofluid_Flow_at_Lower_Stagnation_ Point_over_a_Solid_Sphere_using_Keller-Box_Method.
11. L. Mardianto, B. Widodo, and D. Adzkiya, "Aliran Konveksi Campuran Magnetohidrodinamik yang Melewati Bola Bermagnet," *Limits J. Math. Its Appl.*, vol. 17, no. 1, pp. 9–18, 2020. https://www.researchgate.net/publication/343394819_Aliran_Konveksi_Campuran_Magnetohidrodinamik_yang_Melewati_Bola_Bermagnet.
12. B. J. Gireesha, M. Umeshaiah, B. C. Prasannakumara, N. S. Shashikumar, and M. Archana, "Impact of nonlinear thermal radiation on magnetohydrodynamic three dimensional boundary layer flow of Jeffrey nanofluid over a nonlinearly permeable stretching sheet," *Phys. A Stat. Mech. its Appl.*, vol. 549, p. 124051, 2020. https://www.sciencedirect.com/science/article/abs/pii/S037843711932240X.
13. S. Rosseland, *Astrophysik: Auf atomtheoretischer grundlage*, vol. 11. Springer-Verlag, 2013. https://www.amazon.com/Astrophysik-Atomtheoretischer-Grundlage-Struktur-Einzeldarstellungen/dp/3662245337.
14. B. Mahanthesh, "Flow and heat transport of nanomaterial with quadratic radiative heat flux and aggregation kinematics of nanoparticles," *Int. Commun. Heat Mass Transf.*, vol. 127, p. 105521, 2021. https://www.sciencedirect.com/science/article/abs/pii/S0735193321004140.
15. F. A. Alwawi, H. T. Alkasasbeh, A. M. Rashad, and R. Idris, "MHD natural convection of Sodium Alginate Casson nanofluid over a solid sphere," *Results Phys.*, vol. 16, p. 102818, 2020. https://www.sciencedirect.com/science/article/pii/S2211379719302992.
16. B. Widodo, M. Abu, and C. Imron, "Unsteady nano fluid flow through magnetic porous sphere under the influence of mixed convection," *in Journal of Physics: Conference Series*, vol. 1153, no. 1, p. 12053, 2019. https://iopscience.iop.org/article/10.1088/1742-6596/1153/1/012053.
17. S. H. M. Yasin, M. K. A. Mohamed, Z. Ismail, and M. Z. Salleh, "MHD free convection boundary layer flow near the lower stagnation point flow of a horizontal circular cylinder in ferrofluid," in *IOP Conference Series: Materials Science and Engineering*, vol. 736, no. 2, p. 22117, 2020. https://iopscience.iop.org/article/10.1088/1757-899X/736/2/022117.
18. H. Haiza, I. I. Yaacob, and A. Z. A. Azhar, "Thermal conductivity of water based magnetite ferrofluids at different temperature for heat transfer applications," in *Solid State Phenomena*, vol. 280, pp. 36–42, 2018. https://www.scientific.net/SSP.280.36.
19. M. Z. Swalmeh, H. T. Alkasasbeh, A. Hussanan, and M. Mamat, "Heat transfer flow of Cu-water and Al2O3-water micropolar nanofluids about a solid sphere in the presence of natural convection using Keller-box method," *Results Phys.*, vol. 9, pp. 717–724, 2018. https://www.sciencedirect.com/science/article/pii/S2211379718301086.
20. T. Cebeci and P. Bradshaw, *Physical and computational aspects of convective heat transfer*. Springer Science & Business Media, 2012.

https://books.google.com/books?hl=id&lr=&id=vj7aBwAAQBAJ&oi=fnd&pg=PA1&dq=T.+Cebeci+and+P.+Bradshaw,+Physical+and+computational+aspects+of+convective+heat+transfer.+Springer+Science+%26+Business+Media,+2012.&ots=4gNYLNd-TW&sig=VVcAQhV4FM0oT7nf1BrG1r0b2b0

21. F. Masdeu, C. Carmona, G. Horrach, and J. Muñoz, "Effect of Iron (III) Oxide Powder on Thermal Conductivity and Diffusivity of Lime Mortar," *Materials (Basel).*, vol. 14, no. 4, p. 998, 2021. https://www.ncbi.nlm.nih.gov/pmc/articles/PMC7924037/.
22. C. J. Kumalasari, "Aliran Fluida Magnetohidrodinamik Mikrokutub yang melalui Bola Berpori Dipengaruhi Oleh Konveksi Campuran dan Medan Magnet." Institut Teknologi Sepuluh Nopember, 2018.

MAGNETOHYDRODYNAMICS NANOFERRO FLUID FLOWS PASSING THROUGH A MAGNETIC POROUS SPHERE UNDER THERMAL RADIATION EFFECT

ORIGINALITY REPORT

22%	15%	17%	8%
SIMILARITY INDEX	INTERNET SOURCES	PUBLICATIONS	STUDENT PAPERS

MATCH ALL SOURCES (ONLY SELECTED SOURCE PRINTED)

1%

★ jurnal.iain-padangsidimpuan.ac.id

Internet Source

Exclude quotes	Off	Exclude matches	Off
Exclude bibliography	Off		